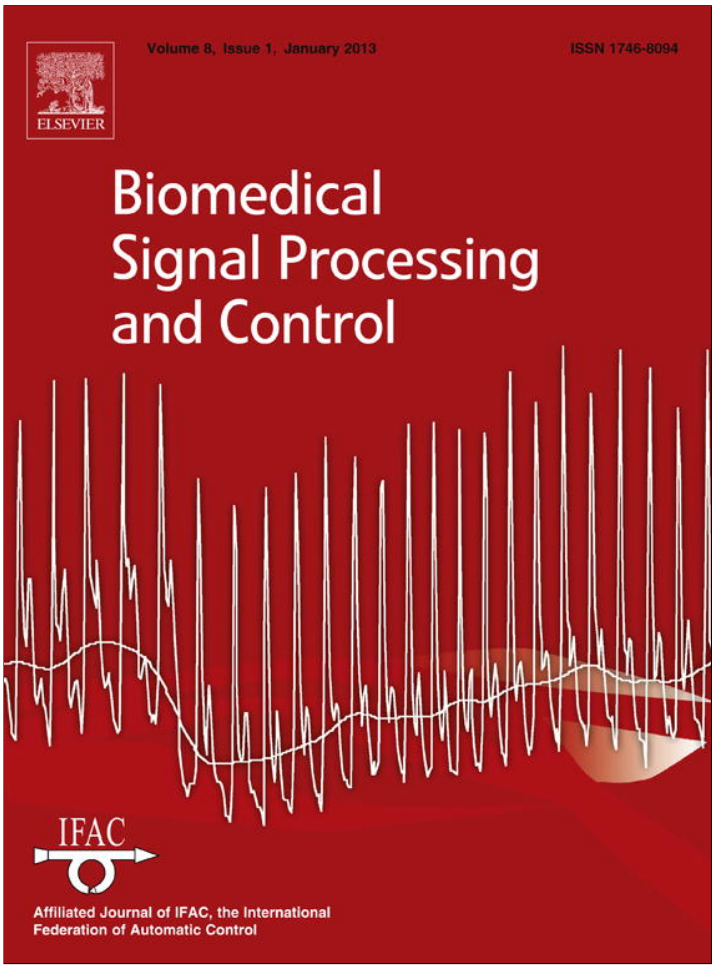

Biomedical Signal Processing and Control 8 (2013) 50–58

Contents lists available at SciVerse ScienceDirect

Biomedical Signal Processing and Control

journal homepage: www.elsevier.com/locate/bspc

3-D warped discrete cosine transform for MRI image compression

K.M.M. Prabhu [a,*,2], K. Sridhar [a,1], M. Mischi [b], H.N. Bharath [a]

[a] Department of Electrical Engineering, IIT Madras, Chennai 600 036, India
[b] Signal Processing Systems Group, Department of Electrical Engineering, Eindhoven University of Technology, 5600 MB Eindhoven, The Netherlands

ARTICLE INFO

Article history:
Received 14 September 2010
Received in revised form 29 March 2012
Accepted 3 April 2012
Available online 30 April 2012

Keywords:
Medical image compression
Discrete cosine transform (DCT)
Warped discrete cosine transform (WDCT)
3-D DCT
3-D WDCT

ABSTRACT

Image compression is an application of data compression on digital images. Several lossy/lossless transform coding techniques are used for image compression. Discrete cosine transform (DCT) is one such widely used technique. A variation of DCT, known as warped discrete cosine transform (WDCT), is used for 2-D image compression and it is shown to perform better than the DCT at high bit-rates. We extend this concept and develop the 3-D WDCT, a transform that has not been previously investigated. We outline some of its important properties, which make it especially suitable for image compression. We then propose a complete image coding scheme for volumetric data sets based on the 3-D WDCT scheme. It is shown that the 3-D WDCT-based compression scheme performs better than a similar 3-D DCT scheme for volumetric data sets at high bit-rates.

1. Introduction

The objective of image compression is to reduce the redundancy of an image data in order to store or transmit data in an efficient manner. There are two basic types of image compression schemes: lossless compression and lossy compression [1–4]. A lossless compression scheme encodes and decodes the data perfectly, and the resulting image matches exactly with the original image. Therefore, there is no degradation or loss of data. Lossless coding techniques include run length encoding, Huffman encoding, entropy coding (Lempel/Ziv), and area coding. Lossy compression schemes, on the other hand, remove redundant and non-essential information that the human eye cannot observe. Typically, with lossy compression schemes, there is a trade-off between compression and image quality. Usually, lossy compression techniques are more complex and require more computations [1,3,4]. The ultimate goal of lossy compression is that the final decompressed image must be visually lossless. The primary focus of this paper is on transform-based coding techniques. More specifically, we are interested in coding schemes which use the discrete cosine transform (DCT) or related transforms [5]. One of the motivations for defining the warped discrete cosine transform (WDCT) is that the DCT fails to compress, if the block of image contains mostly high frequencies [6,7]. The warped discrete Fourier transform (WDFT) computes the frequency samples of the discrete-time Fourier transform (DTFT) at unequally spaced frequency points [8].

In this paper, we extend this concept to an adaptive discrete cosine transform referred to as WDCT, which computes the DCT samples by warping the frequency axis by means of an all-pass transform [6]. The WDCT can be implemented as a cascade of DCT and an infinite impulse response (IIR) all-pass filter whose parameter is used to adjust the transform according to the frequency contents of the input signal [5,6,9]. More precisely, the input signal is warped by an all-pass function in such a way that it has a frequency distribution which is suitable for coding. We can represent the WDCT by a single matrix, similar to the DCT. For example, when there are only eight samples in a block, the output of an IIR filter can be represented by a linear combination of the first eight samples of the impulse response of the IIR filter transfer function. Thus, the outputs of all-pass filters can be represented by the multiplication of a known matrix with the input vector. Yet another way of implementing WDCT is by interpreting DCT as a filter bank [6]. In this paper we have used the filter bank approach to implement WDCT. This approach is explained in Section 3 of the paper.

This paper is organized as follows. In Section 2, we discuss the DCT-based coding schemes. In Section 3, we briefly introduce the 1-D version of the WDCT and extend this concept to 2-D and 3-D versions. The properties of WDCT are outlined and a detailed explanation concerning encoder complexity is discussed. Section 4 explains the encoding and decoding schemes used in the

* Corresponding author.
E-mail addresses: prabhu@ee.iitm.ac.in, prabhu_kmm@hotmail.com (K.M.M. Prabhu), sidhuee@gmail.com (K. Sridhar), M.Mischi@tue.nl (M. Mischi), hn.bharath@gmail.com (H.N. Bharath).
[1] Presently with Verizon Data Services India Private Limited, Chennai 600 032, India.
[2] Earlier at Signal Processing Systems Group, Department of Electrical Engineering, Eindhoven University of Technology, 5600 MB Eindhoven, The Netherlands.

1746-8094/$ – see front matter © 2012 Elsevier Ltd. All rights reserved.
http://dx.doi.org/10.1016/j.bspc.2012.04.004

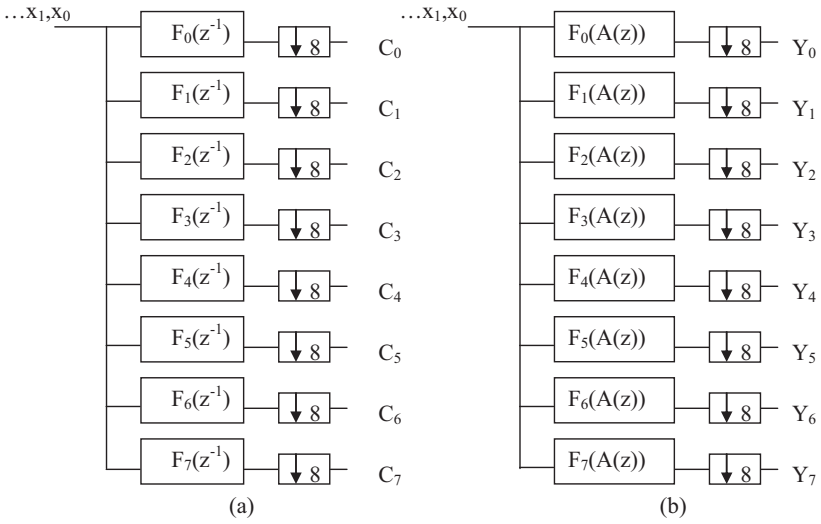

Fig. 1. (a) DCT Filter bank and (b) WDCT Filter bank.

algorithm. The results are analyzed in Sections 5 and 6 presents the conclusions.

2. DCT-based coding schemes

The essential steps involved in typical transform-based encoding and decoding schemes include transformation, quantization and entropy coding at the encoder and the corresponding inverse operations at the decoder.

The DCT is a popular transform used for image compression due to its energy compaction property. The most commonly used DCT in image coding is the Type-II DCT [6], which is defined as follows:

$$C_k = U(k) \sum_{n=0}^{N-1} x_n \cos\left(\frac{(2n+1)k\pi}{2N}\right), \quad k = 0,\ 1, \ldots, N-1 \qquad (1)$$

with C_ks and x_ns being the DCT coefficients and input samples, respectively. $U(k)$ is defined in Section 3.

In this paper, we are interested in the compression of magnetic resonance imaging (MRI) data. Though medical images are usually compressed using lossless coding techniques, there are several applications where lossy compression is acceptable as long as the image quality is not degraded [10]. The DCT-based schemes make use of the fact that there is a high correlation between adjacent pixels, in order to compress the data. DCT de-correlates this correlation between adjacent pixels, which results in a considerable number of coefficients becoming zero. After quantization, we can code these coefficients very efficiently using entropy coding.

However, there are several other transforms like the DCT which also have similar energy compaction properties [11]. The warped discrete cosine transform (WDCT) is one such transform [8]. It has been shown that WDCT outperforms DCT for high bit-rate operations [6]. In this paper, we extend this concept to three dimensions. It has been shown that 3-D DCT performs better than all the other coding schemes (especially for MRI data) for high bit-rate operations [3]. We also know that the 2-D WDCT performs better than 2-D DCT for high bit-rates [6,7]. Therefore, we have combined these two ideas to improve the coding performance of MRI images at high bit-rate operations, by proposing a new technique that uses the 3-D version of the WDCT. In this paper we define the 3-D WDCT and propose a complete image encoding and decoding scheme based on this. The performance of this algorithm is compared with a scheme that uses the 3-D DCT.

The DCT basis functions for an 8×8 image can be represented as a matrix of basis functions [12]. The higher frequency components tend to have lower values when the DCT is performed, while the lower frequency components have higher values.

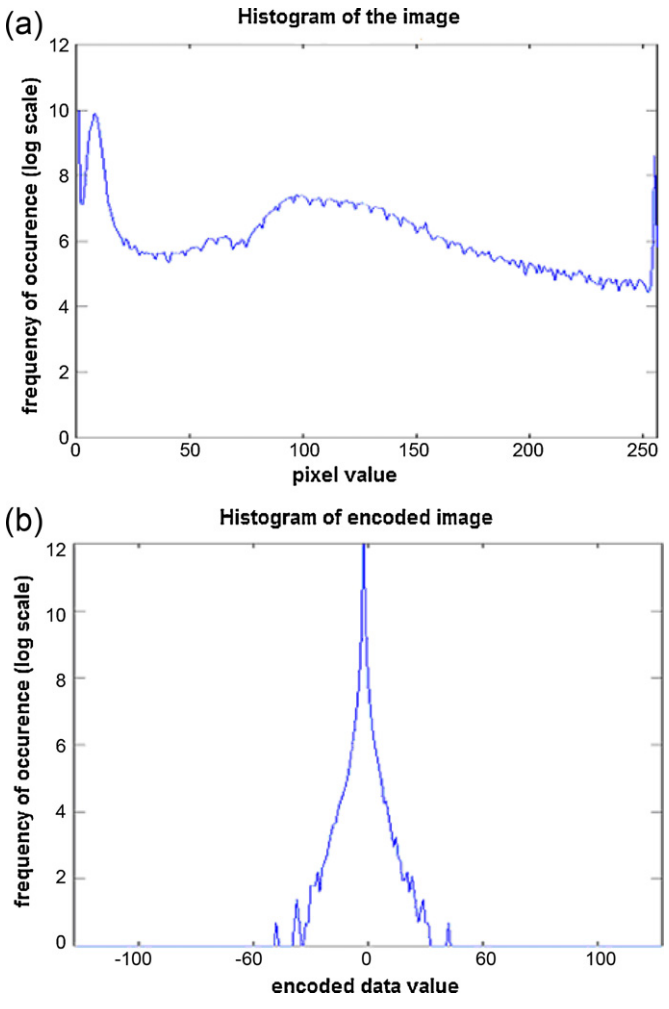

Fig. 2. (a) Histogram of original image (log scale). (b) Histogram of encoded data (log scale).

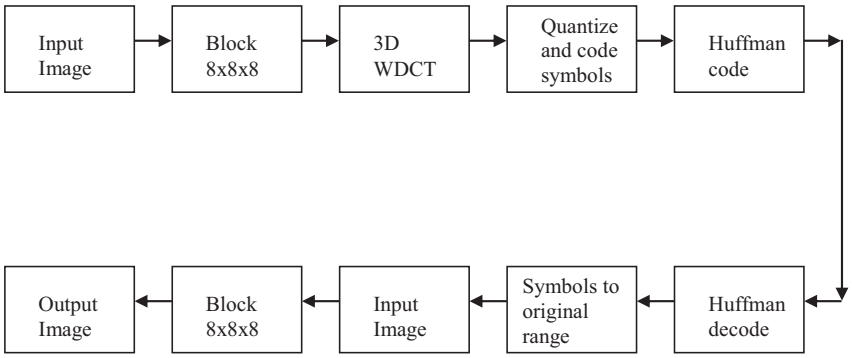

Fig. 3. Block diagram of 3-D WDCT encoding and decoding schemes.

3. Warped discrete cosine transform (WDCT)

In this section we briefly explain the implementation of WDCT using the filter bank approach. In this approach the DCT matrix can be considered as a filter bank consisting of eight FIR filters, with eight taps each. We define an 8-point 1-D DCT of the input vector $[x_0\, x_1\, x_2\, x_3\, x_4\, x_5\, x_6\, x_7]^T$ as

$$C_k = U(k) \sum_{n=0}^{7} x_n \cos\left(\frac{(2n+1)k\pi}{16}\right), \quad \text{for} \quad k = 0,\ 1,\ 2, \ldots, 7 \quad (2)$$

where

$$U(k) = \begin{cases} \dfrac{1}{2\sqrt{2}}, & k = 0 \\ \dfrac{1}{2}, & \text{otherwise} \end{cases}.$$

The DCT of the input vector is computed using a filter bank as indicated in Fig. 1(a). The block referred to as DCT filter bank computes the DCT for every input block and the DCT filter coefficients can be represented as follows:

$$F_k(z^{-1}) = U(k) \left\{ \cos\frac{k\pi}{16} + \cos\frac{3k\pi}{16} z^{-1} + \cdots + \cos\frac{15k\pi}{16} z^{-7} \right\}. \quad (3)$$

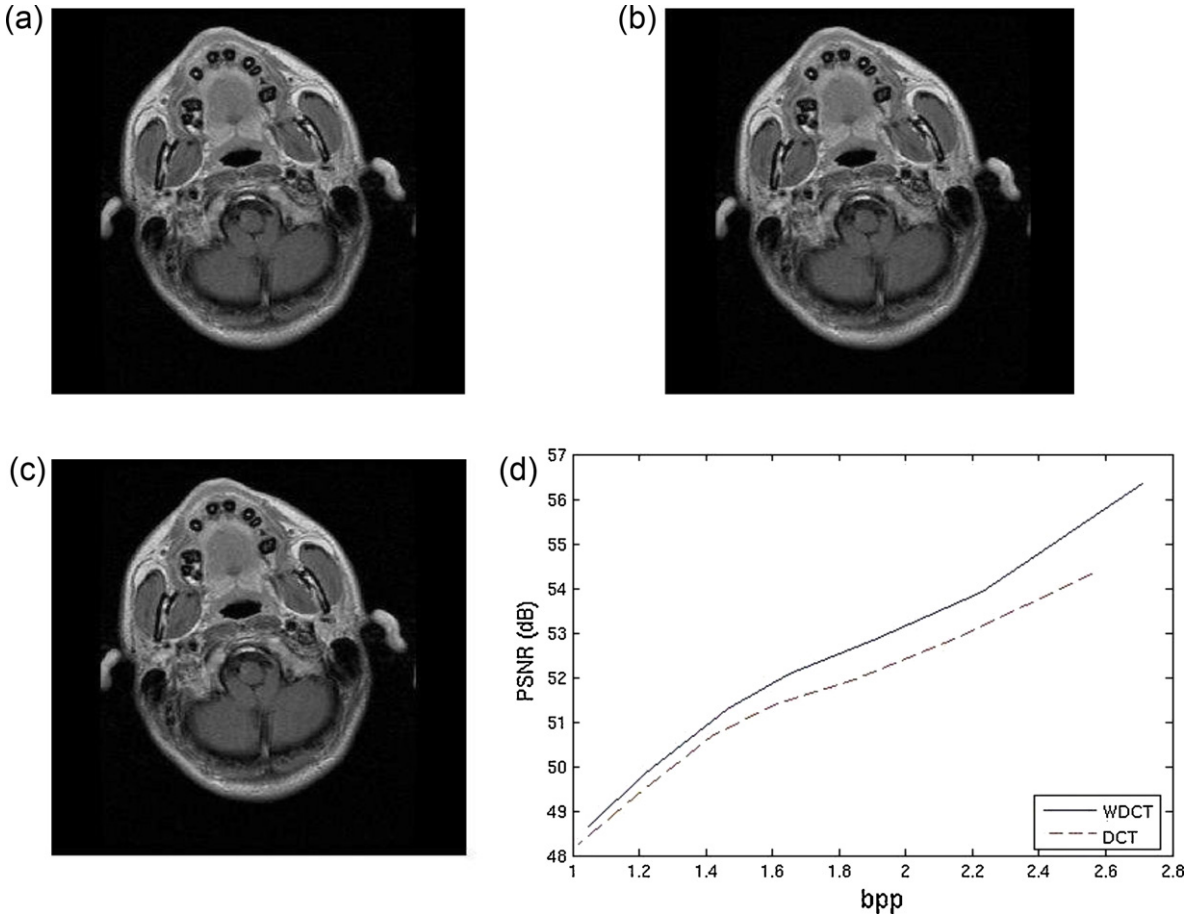

Fig. 4. (a) 3-D DCT reconstructed image (PSNR = 54.38, bpp = 2.57), (b) 3-D WDCT reconstructed image (PSNR = 56.36, bpp = 2.70), (c) original image and (d) PSNR vs. bpp plot.

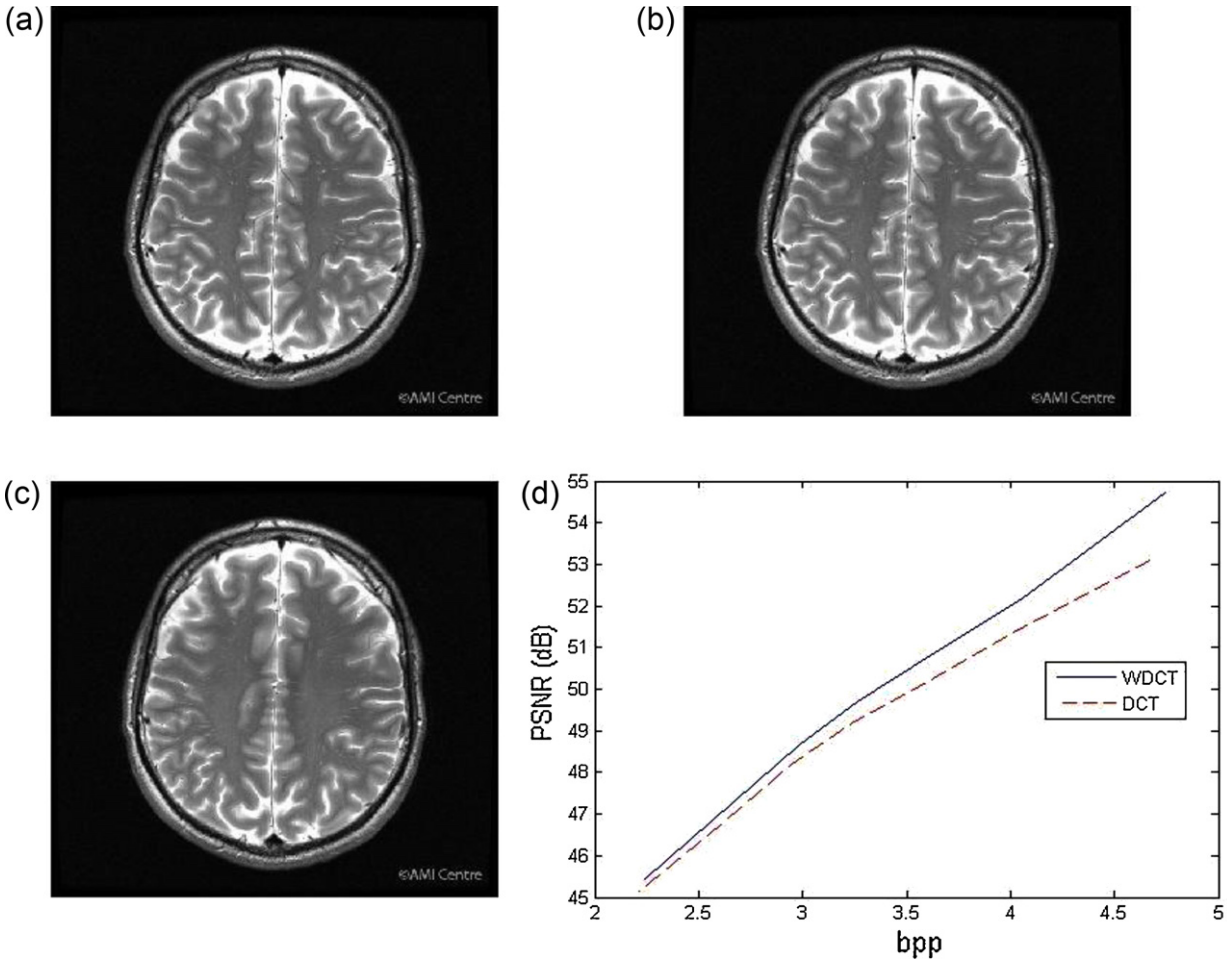

Fig. 5. (a) 3-D DCT reconstructed image (PSNR = 53.17, bpp = 4.70), (b) 3-D WDCT reconstructed image (PSNR = 55.72, bpp = 4.74), (c) original image and (d) PSNR vs. bpp plot.

The conventional DCT filter bank works well for inputs with mostly low frequency components. However, for inputs with high frequency components, the magnitudes of the outputs from $F_k(z^{-1})$ for higher values of k is large, which degrades the coding efficiency. However, higher magnitudes will increase the sample values. As a result, a larger Huffman code table must be used. This in turn increases average code length per symbol, due to which there is degradation in its efficiency. Therefore, in WDCT we use a filter bank whose frequency response can be adjusted according to the frequency content of the inputs.

The combination of all-pass IIR filter and the DCT can be considered as another filter bank with eight IIR filters. This is obtained by warping the frequency response of the FIR filters. For warping the frequency response of the filter bank given in Fig. 1(a), a suitable transform is obtained by replacing z^{-1} by an all-pass filter, $A(z)$ (as shown in Fig. 1(b)).

$$A(z) = \frac{-\alpha + z^{-1}}{1 - \alpha z^{-1}}. \tag{4}$$

Here α is used as the control parameter for warping the frequency response. $A(z)$ is known as the Laguerre filter and is widely used in other applications [13]. The resulting warped DCT filter bank is shown in Fig. 1(b), where $F_k(z^{-1})$ have been now replaced with IIR filters given by

$$F_k(A(z)) = \sum_{n=0}^{7} U(k) \cos\frac{(2n+1)k\pi}{16}(A(z))^n, \tag{5}$$

that is,

$$F_k(A(z)) = U(k)\left\{\cos\frac{k\pi}{16} + \cos\frac{3k\pi}{16}A(z) + \cdots + \cos\frac{15k\pi}{16}(A(z))^7\right\}. \tag{6}$$

By finding the truncated or approximated FIR filter coefficients for these IIR filters, the WDCT filter bank can be represented by a single matrix. The approximate 8 tap FIR filter is obtained by taking the inverse discrete Fourier transform (IDFT) of the sampled values of $F_k(A(e^{j\omega}))$, at $\omega = 0, (2\pi/8), (4\pi/8), \ldots, (14\pi/8)$. The WDCT is similar to the DCT, except that the primary focus in WDCT is on finding an all-pass function that minimizes the mean square error (MSE). The filter bank using this all-pass function is the basis for the WDCT algorithm. Although this would lead to additional computations on the encoder block, the WDCT coefficients thus obtained provide better encoding.

3.1. 3-D DCT and WDCT

We define the 3-D DCT of the three dimensional matrix x as follows:

$$C(k_1, k_2, k_3) = U(k_1)U(k_2)U(k_3)\sum_{n_1=0}^{N-1}\sum_{n_2=0}^{N-1}\sum_{n_3=0}^{N-1} x(n_1, n_2, n_3)D_{k_1,n_1}D_{k_2,n_2}D_{k_3,n_3}, \tag{7}$$

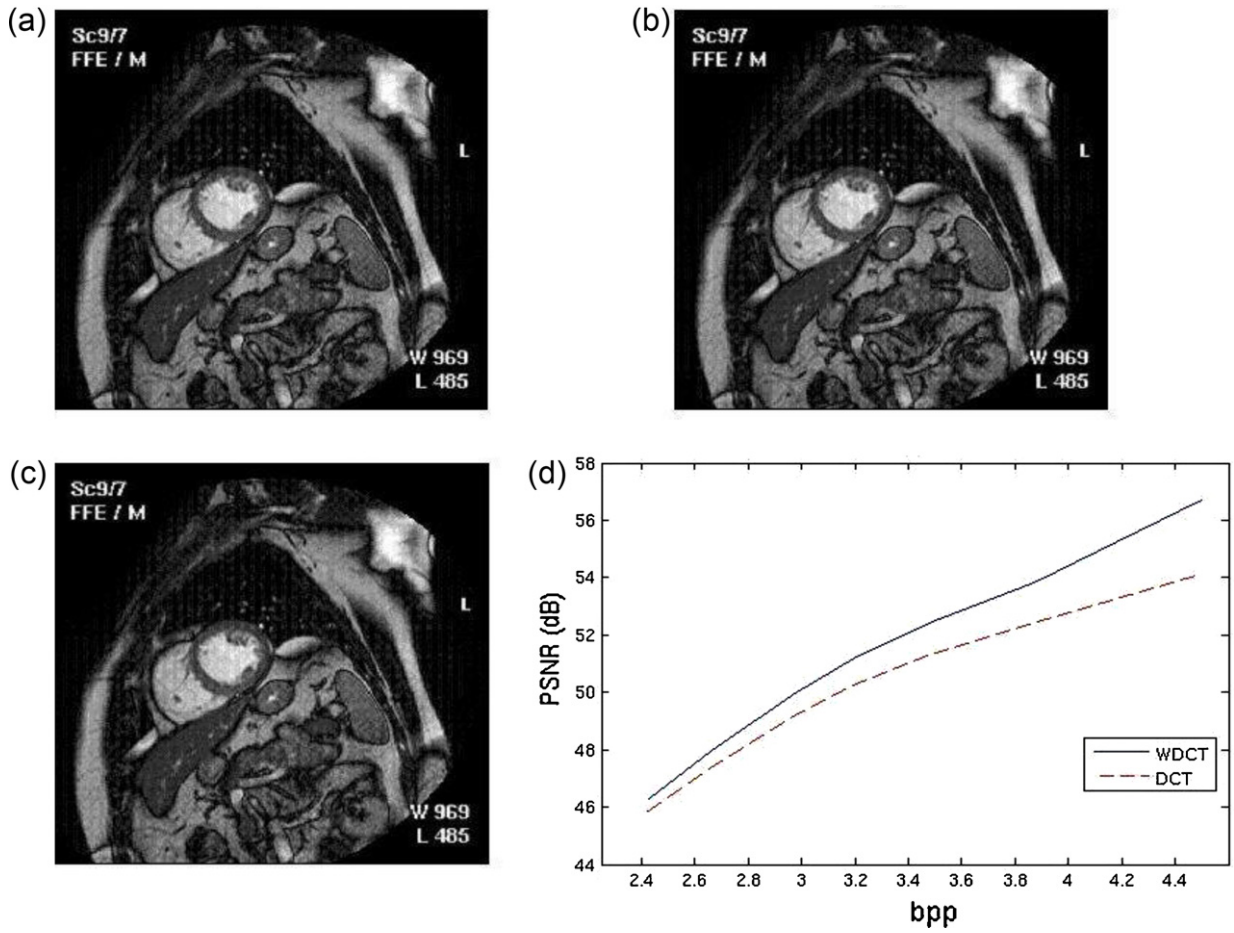

Fig. 6. (a) 3-D DCT coded and reconstructed image (PSNR = 52.40, bpp = 3.86), (b) 3-D WDCT coded and reconstructed image (PSNR = 53.84, bpp = 3.87), (c) original image and (d) PSNR vs. bpp plot.

where a general D_{k_i,n_i} is defined as

$$D_{k_i,n_i} = \cos\left(\frac{(2k_i+1)n_i\pi}{2N}\right), \quad \text{for} \quad i=0 \quad \text{to} \quad N-1$$

and

$$U(k_i) = \begin{cases} \frac{1}{\sqrt{N}}, & k=0 \\ \sqrt{\frac{2}{N}}, & \text{otherwise} \end{cases}, \quad \text{for} \quad i=1,\ 2,\ 3.$$

Eq. (7) is an extension of the existing 2-D DCT to the 3-D DCT domain. The 3-D DCT is explained in [5]. Similarly, 3-D WDCT can also be expressed as in Eq. (7), which is given below

$$W(k_1,k_2,k_3) = \sum_{n_1=0}^{N-1}\sum_{n_2=0}^{N-1}\sum_{n_3=0}^{N-1} x(n_1,n_2,n_3) M_{k_1,n_1} M_{k_2,n_2} M_{k_3,n_3}. \quad (8)$$

Here M_{k_i,n_i} does not have closed-form expression as in the case of DCT, and the kth row of M represents the filter coefficients of the 8-tap FIR filter approximation of $F_k(A(z))$. The properties of 3-D WDCT discussed in the next section fructify our evaluation of 3-D WDCT as an algorithm superior to the 3-D DCT.

3.2. 3-D WDCT properties

The principal advantage of image transformation is the removal of redundancy in between the neighboring pixels. This leads to uncorrelated transform coefficients which can be encoded independently. The 3-D DCT and 3-D WDCT have excellent de-correlation properties, due to which a large number of coefficients become zero.

(1) **Energy compaction**: The efficacy of a transform scheme can be directly evaluated by its ability to pack the data into as few coefficients as possible. This allows the quantizer to discard coefficients with relatively small amplitudes, without introducing visual distortion in the reconstructed image. The 3-D WDCT exhibits excellent energy compaction properties for highly correlated images. In order to understand the energy compaction property of the 3-D WDCT, the histograms of the image and that of the transformed coefficients are considered. The histogram of the original image and that of the transformed coefficients using WDCT are shown in Fig. 2(a) and (b), respectively. From these figures, it can be observed that all the values in the range [0, 255] occur almost uniformly in the original image (Fig. 2(a)), and therefore the energy is spread out across all the pixel values. However, for the encoded (transformed) data, many coefficients are zero as shown in Fig. 2(b), and therefore most of the energy is packed only in few coefficients [11]. This provides a strong support to our claim that 3-D WDCT has good de-correlation and energy compaction properties.

(2) **Separability**: Eq. (8), which is the representation of WDCT, can also be written as

$$W(k_1,k_2,k_3)$$

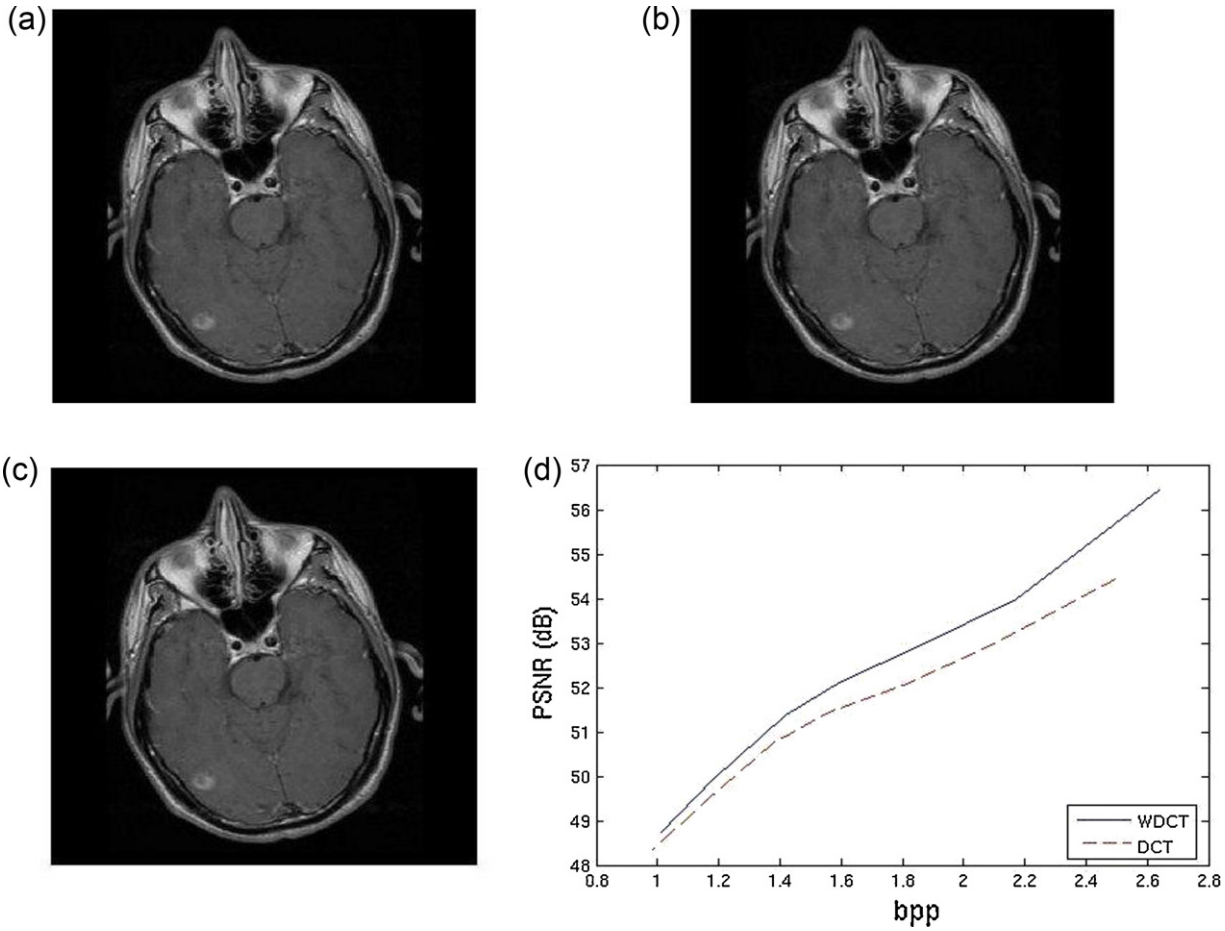

Fig. 7. (a) 3-D DCT reconstructed image (PSNR = 54.48, bpp = 2.51), (b) 3-D WDCT reconstructed image (PSNR = 56.43, bpp = 2.61), (c) original image and (d) PSNR vs. bpp plot.

$$= \sum_{n_1=0}^{7} M_{k_3,n_3} \left[\sum_{n_2=0}^{7} M_{k_2,n_2} \left\{ \sum_{n_3=0}^{7} M_{k_1,n_1} x(n_1, n_2, n_3) \right\} \right]. \quad (9)$$

Therefore, the 3-D WDCT equation is separable and we can compute the 3-D WDCT as a cascade of three 1-D WDCT computations. This involves the following four steps:

- The 8-point row wise WDCT of the image is computed.
- The 8-point column wise WDCT of the image is computed.
- Eight such matrices are stacked.
- The WDCT is performed in the third dimension.

4. 3-D WDCT encoding and decoding

The complete encoding and decoding schemes are shown in Fig. 3.

The input volumetric data consists of a set of MRI grayscale images. First, we form stacks of 8 images from the data. In fact, for MRI images that are acquired by a standard 1.5 T scanner, 8 samples correspond typically to a physical distance between 1 and 2 cm, depending on the specific MRI setting. Each of these stacks is then further divided into blocks of $8 \times 8 \times 8$. We have three reasons for choosing such a block size:

(a) It is more convenient to compute the 8-point WDCT, since 8 is a power of 2.

(b) If the block size is very small, it under-utilizes correlation between adjacent pixels, whereas if the block size is very large correlation is small and consequently the energy compaction would be poor. Therefore, a block size of $8 \times 8 \times 8$ turns out to be a good compromise.

(c) We can choose a single all-pass parameter for the entire block. The correlation properties of the MRI image set are similar in the *x*, *y* and *z*-directions (unlike in the case of 3-D data sets like video). Hence, choosing a symmetrical block such as $8 \times 8 \times 8$ makes sense. If we had chosen only an un-symmetrical block such as $6 \times 8 \times 10$, we would have to choose different all-pass parameters for each direction and they will have to be transmitted separately. This would result in considerable overhead in the number of transmitted bits, without any significant improvement in the image quality.

4.1. Encoder

The 3-D WDCT encoder uses the separability property of the 3-D WDCT (discussed in Section 3). The 3-D WDCT is implemented as a sequence of three 1-D WDCT computations. We first take an 8×8 (x–y plane) image out of the $8 \times 8 \times 8$ block, and compute the 2-D WDCT by pre-multiplying and post-multiplying the 2-D image matrix by the W_{WDCT} matrix and its transpose, respectively, i.e., $W_{\text{2-D WDCT}} = M_{\text{WDCT}} X M^T{}_{\text{WDCT}}$, where M_{WDCT} is the 1-D WDCT matrix and X is the 8×8 image. We perform this matrix multiplication for each of the eight 8×8 images. We then compute 1-D WDCT along the z-direction by taking 8-element vectors and pre-multiplying them by the WDCT matrix.

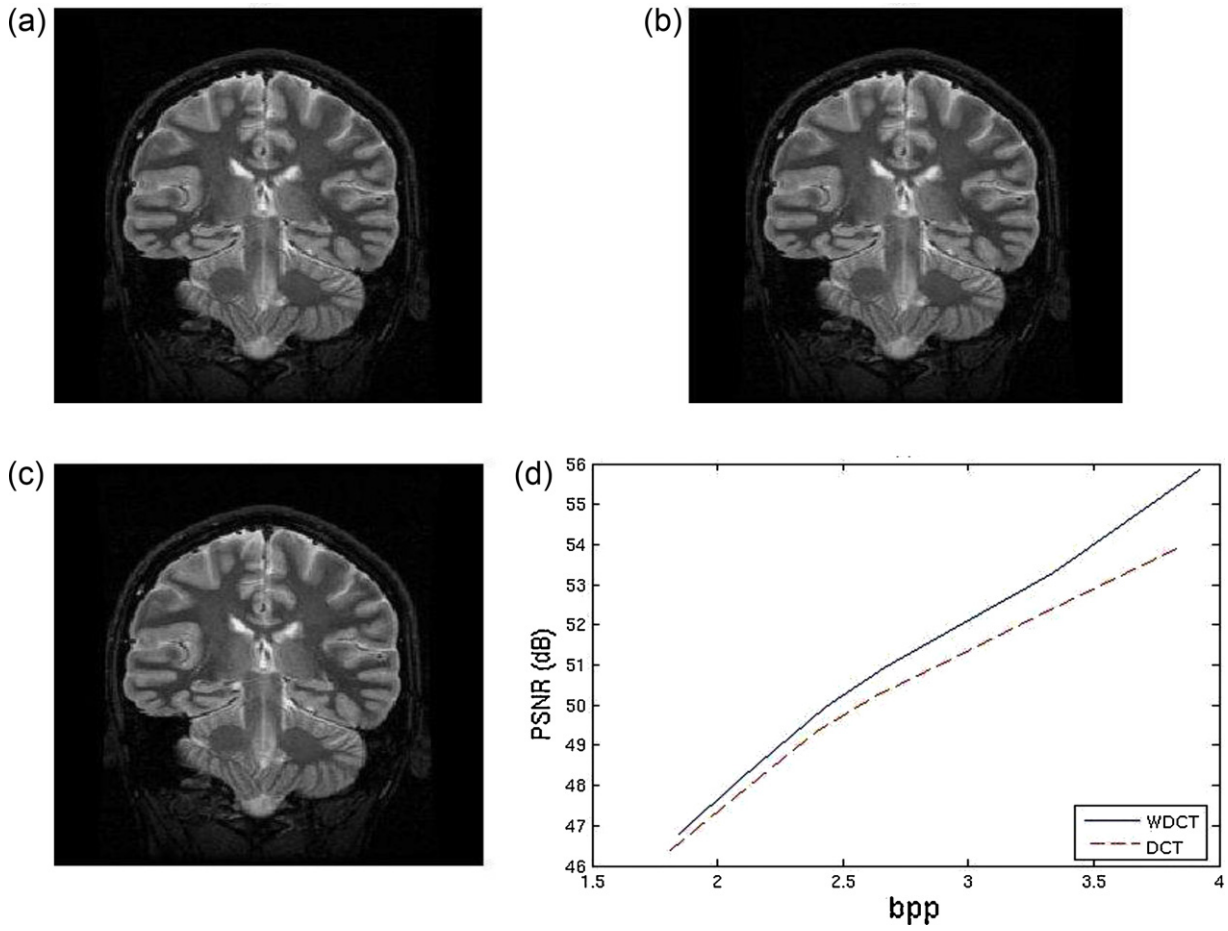

Fig. 8. (a) 3-D DCT coded and reconstructed image (PSNR = 53.94, bpp = 3.85), (b) 3-WDCT coded and reconstructed image (PSNR = 55.85, bpp = 3.92), (c) original image and (f) PSNR vs. bpp plot.

The 3-D WDCT encoder not only performs the 3-D WDCT computation, but also finds the optimal α which minimizes the reconstruction error after quantization. The mean square error (MSE) is given by

$$\text{MSE} = \frac{1}{8^3}\sum_{n_1=0}^{7}\sum_{n_2=0}^{7}\sum_{n_3=0}^{7}[X(n_1,n_2,n_3) - X^R(n_1,n_2,n_3)]^2. \quad (10)$$

The algorithm used by the 3-D WDCT encoder is summarized in the following six steps:

1. Quantize α into L steps in the range $[-0.1, 0.1]$.
2. Form n WDCT matrices, denoted by WDCT_n for $n = 1$ to L.
3. For each block, perform WDCT_n, quantization and inverse WDCT for $n = 1$ to L.
4. Choose WDCT_n that minimizes the reconstruction error and store the index n.
5. Quantize the block transformed by WDCT_n, encode by Huffman coding and transmit.
6. Repeat steps 3–5 for each block.

4.1.1. Quantization and Huffman coding

The 3-D WDCT increases the dynamic range of the input data from its original range. It is desirable to perform quantization by dividing the transformed coefficients by a quantization value. In JPEG algorithm, different quantization values are used: the low-frequency coefficients are divided by smaller values while the high-frequency coefficients are divided by larger values. In this paper, we have used only two quantization values, one for the DC coefficients and the other for all the AC coefficients. The DC quantization value is kept fixed and the bpp is varied by varying the AC quantization values. A higher quantization value will result in high compression, i.e., lower bpp, but that would result in a poorer image quality. Therefore, quantization value is a trade-off between image quality and the bit-rate. De-quantization can be simply done by multiplying the quantized coefficient by the quantization value.

After the quantization process, we code the data using an entropy coding scheme, such as Huffman coding. In order to take advantage of the sparsity of the transformed data, the encoded 3-D block is converted back to 1-D by doing a 3-D zigzag scan, which creates a long sequence of zeros at the end. This large sequence of continuous zeros is formed by the higher frequency components. Run length encoding is performed on this sequence, as it is done in a standard JPEG compression. Huffman encoding is performed separately on DC and AC coefficients. In the case of DC coefficients, the difference between the two is encoded rather than using the actual value. However, for AC coefficients, no such differential encoding is necessary. Huffman encoding is performed using standard Huffman table in baseline sequential encoding mode, as in the JPEG standard. At the decoder end, we perform Huffman decoding to obtain quantized coefficients. Then, the de-quantization is done and finally the $8 \times 8 \times 8$ (3-D) image block is reconstructed by taking the inverse 3-D WDCT transform.

4.1.2. Inverse 3-D WDCT

In order to find the inverse 3-D WDCT from the $8 \times 8 \times 8$ encoded block, we do the following.

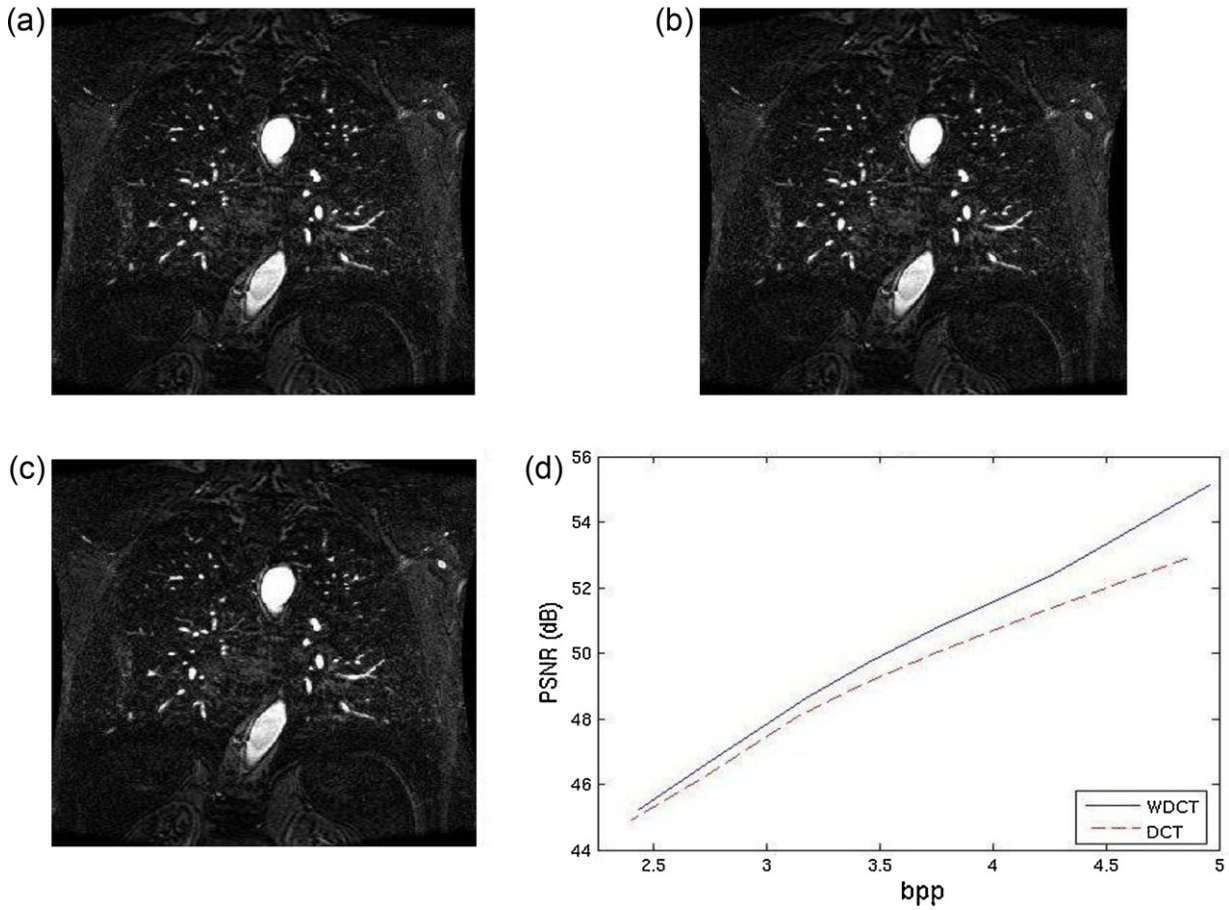

Fig. 9. (a) 3-D DCT reconstructed image (PSNR = 51.22, bpp = 4.20), (b) 3-D WDCT reconstructed image (PSNR = 52.33, bpp = 4.25), (c) original image and (d) PSNR vs. bpp plot.

1. We compute the inverse WDCT (IWDCT) matrices corresponding to different values of α.
2. We then pick that IWDCT matrix which corresponds to the value of α received from the encoder and multiply all the 8-element vectors in the z-direction by this matrix. We then divide the block into eight sets of 8×8 (x–y plane) images.
3. We pre-multiply and post-multiply each of these images by IWDCT and its transpose, respectively, to obtain the reconstructed images, i.e., find $X_{2\text{-D IWDCT}} = W_{\text{IWDCT}}\, Y\, W^{T}_{\text{IWDCT}}$, where W_{IWDCT} is the IWDCT matrix, Y is the encoded data and $X_{2\text{-D IWDCT}}$ is the 8×8 decoded image.

It is important to note that the complexity of the decoder is much less than that of the encoder. In the decoder, there is only a single 3-D IWDCT computation. The complexity of a 3-D WDCT decoder is comparable to that of DCT-based decoders. However, we have an increased complexity at the encoder end when compared to the DCT-based encoders, where there is only one set of matrix multiplications. The improved performance by using 3-D WDCT comes at the expense of increased computational complexity at the encoding end.

5. Results and discussion

The input to the 3-D WDCT coding scheme is a set of grayscale MRI images. The output of the encoder end is a stream of bits, which is fed back to the decoder. The output of the decoder is the reconstructed image set. For simplicity, we assume that the data sets are in multiples of 8. The values of the different parameters used are: (i) number of levels of α is 16, (ii) range of $\alpha = [-0.1, 0.1]$, (iii) size of the individual images = 512×512 or 256×256 and (iv) range of input data: [0, 255].

We use the peak signal-to-noise ratio (PSNR) as a measure of the image quality [14]:

$$\text{PSNR} = 10\ \log_{10}\left(\frac{\text{MAX}_I{}^2}{\text{MSE}}\right) = 20 \log_{10}\left(\frac{\text{MAX}_I}{\sqrt{\text{MSE}}}\right), \tag{11}$$

where MAX_I is the maximum pixel value of the input image.

In the rest of this section, we present several results obtained of applying our algorithm for compression of real MRI images. The MRI images presented in Figs. 4(a) and 5(a) are projections of the human brain at various rotations [15]. Fig. 6(a) shows the MRI image set of cardiopulmonary vasculature [16]. The MRI images presented in Figs. 7(a) and 8(a) are projections of human head at various rotations [17].

Fig. 4 shows an original MRI scan of the brain and the results when we apply the 3-D DCT and 3-D WDCT algorithms on this image set.

In Fig. 5, at a bpp of 4, the PSNR for the 3-D WDCT reconstructed image is 52.17 dB, whereas the PSNR for the 3-D DCT reconstructed image is 51.37 dB. Therefore, there is an improvement of about 0.8 dB in the PSNR level, which makes the 3-D WDCT superior to the 3-D DCT algorithm.

The original image set in Fig. 6 is an MRI image set of the short axis of the heart. Several planes are taken and for each plane, a cardiac cycle is imaged.

In Fig. 7, at a bpp of 2.6, the PSNR for the 3-D DCT reconstructed image is 54.5 dB, while the corresponding PSNR for the 3-D WDCT is 56.4 dB. Therefore, there is an improvement of about 2 dB.

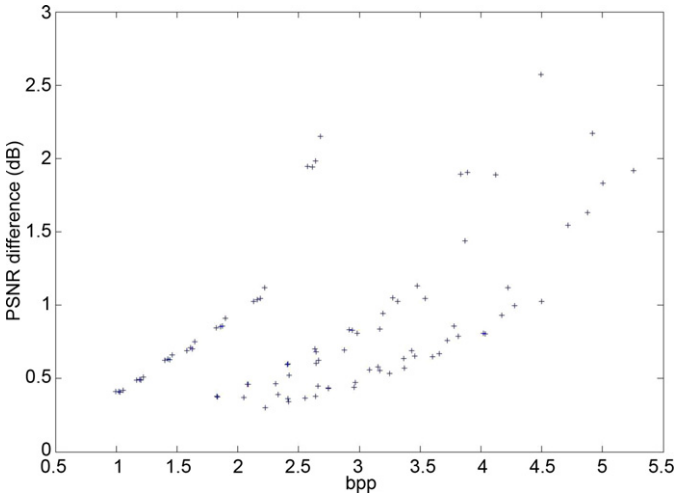

Fig. 10. PSND (difference in dB) between 3-D WDCT and 3-D DCT as a function of bpp.

Fig. 8 shows an original MRI image set of size 256 × 256 and the results when we apply the 3-D DCT and 3-D WDCT algorithms on this image set.

Fig. 9(a) gives an MRI angiography which shows coronal slices acquired from consecutive anteroposterior positions within the torso. The study was performed on a 1.5 T General Electric (GE) Signa imaging system with gadolinium-contrast-enhancement for visualization of the cardiopulmonary vasculature. The pulse sequence used was a 3-D time-of-flight fast spoiled gradient recalled acquisition in steady state (FSPGR, TR = 6.3, TE = 1.4, NEX = 1, FOV = 40 cm, slice thickness = 1.2 mm) [16].

The plot in Fig. 10 summarizes the results for the complete adopted dataset, comprising 13 different image sets. The difference between the PSNR values obtained using 3-D WDCT and 3-D DCT is called as PSND, which is expressed in dB. We have plotted PSND as a function of bpp (average of WDCT and DCT). Average of bpp is taken because for a given quantization value, there will be slight differences between the bpp of 3-D WDCT and the bpp of 3-D DCT. On an average, it can be noticed how 3-D WDCT outperforms 3-D DCT for higher bpp.

6. Conclusions and future directions

In this paper, we have defined and developed the 3-D WDCT, a transform that has not been previously investigated in the literature. Although the 3-D WDCT is based on the properties of 2-D WDCT, this work is the first attempt in exploring the efficacy of the 3-D WDCT algorithm. The important properties of this transform, which make it especially suitable for image compression, have been discussed. We have proposed a complete image coding scheme for volumetric data sets based on the 3-D WDCT. The algorithms used by each of the blocks of the encoder and decoder have also been presented.

The performance of this scheme is compared with that of a similar 3-D DCT scheme, using 'PSNR vs. bpp' plots. From the results obtained, which are summarized in Fig. 10, we observe that the 3-D WDCT performs better than the 3-D DCT for high bit-rate operations (above 2 bpp for majority of the examples).

The all-pass filter that we have used in the WDCT algorithm is the key to the performance enhancement. Although this adds to the complexity on the encoder side, our results are assertive enough to compensate for this additional overhead. It is imperative that we use high bit-rates for such images, so that there is no serious degradation of image quality. Since it has been already established that the performance of 3-D DCT on MRI images is better than all the other algorithms for high bit-rates, our findings therefore validate the claim that the proposed 3-D WDCT method yields a better performance among all the coding schemes. We hope our work will generate enough interest in probing further for more efficient algorithms to compress MRI images. In our algorithm, we have explored only one way of finding an efficient all-pass filter that minimizes the MSE. Further research can be carried out in finding more effective constraints which could improve the performance. The results presented in this paper provide enough evidence to conclude that 3-D WDCT is an efficient algorithm in compressing MRI images (when compared to the 3-D DCT) at higher bit-rates. Eventually, we hope that there is a possibility of 3-D WDCT replacing 3-D DCT as the most widely used compression algorithm for MRI images in the future.

Acknowledgments

The authors wish to thank Mr. Rohit K. Reddy for initiating the work presented here. The authors also profusely thank the two anonymous reviewers for their critical comments and suggestions which have greatly improved the quality and presentation of the paper.

References

[1] A.K. Jain, Image data compression: a review, Proceedings of the IEEE 69 (3) (1981) 349–389.
[2] G.P. Abousleman, M.W. Marcellin, B.R. Hunt, Compression of hyperspectral imagery using the 3-D DCT and hybrid DPCMDCT, IEEE Transactions on Geoscience and Remote Sensing 33 (1995) 26–34.
[3] Z. Xiong, X. Wu, S. Cheng, J. Hua, Lossy-to-lossless compression of medical volumetric data using three-dimensional integer wavelet transforms, IEEE Transactions on Medical Imaging 22 (2003) 459–470.
[4] P. Schelkens, A. Munteanu, J. Barbarien, M. Galca, X.G. Nieto, J. Cornelis, Wavelet coding of volumetric medical datasets, IEEE Transactions on Medical Imaging 22 (2003) 441–458.
[5] S.C. Tai, Y.G. Wu, C.W. Lin, An adaptive 3-D discrete cosine transform coder for medical image compression, IEEE Transactions on Information Technology and Biomedicine 4 (2000) 259–263.
[6] N.I. Cho, S.K. Mitra, Warped discrete cosine transform and its application in image compression, IEEE Transactions on Circuits and Systems for Video Technology 10 (2000) 1364–1373.
[7] I.K. Kim, N.I. Cho, S.K. Mitra, Rate-distortion optimization of the image compression algorithm based on the warped discrete cosine transform, Signal Processing 83 (9) (2003) 1919–1928.
[8] A. Makur, S.K. Mitra, Warped discrete-Fourier transform: theory and applications, circuits and systems I: fundamental theory and applications, IEEE Transactions on 48 (September (9)) (2001) 1086–1093.
[9] O. Urhan, S. Ertürk, Parameter embedding mode and optimal post-process filtering for improved WDCT image compression, IEEE Transactions on Circuits and Systems for Video Technology 18 (2008) 528–532.
[10] G. Menegaz, J.P. Thiran, Lossy to lossless object-based coding of 3-D MRI data, IEEE Transactions on Image Processing 11 (2003) 1053–1062.
[11] J.H. Chang, Warped discrete cosine transform-based noisy speech enhancement, IEEE Transactions on Circuits and systems 52 (2005) 535–539.
[12] D. Marshall, The Discrete Cosine Transform (DCT), http://www.cs.cf.ac.uk/Dave/Multimedia/node231.html (last accessed on 24.05.11).
[13] G. Evangelista, S. Cavaliere, Discrete frequency warped wavelets: theory and applications, IEEE Transactions on Signal Processing 46 (1998) 874–884.
[14] T.H. Oh, R. Besar, Image quality measures of compressed medical images, in: 4th National Conference on Telecommunication Technology Proceedings, Shah Alam, Malaysia, 2003.
[15] Advanced Magnetic Imaging Centre, AMI Centre, Aalto University, http://ami.tkk.fi/en/facilities/example_images/brain/t2_fse-xl/ (last accessed on 20.01.12).
[16] G. Holmvang, PhysioBank: Samples of MR Images, http://physionet.cps.unizar.es/physiobank/database/images/ (last accessed on 20.01.12).
[17] John Hall's Home Page, http://overcode.yak.net/15 (last accessed on 20.01.12).